

Efficient Long-Horizon Vision-Language-Action Models via Static-Dynamic Disentanglement

Weikang Qiu¹ Tinglin Huang¹ Aosong Feng¹ Rex Ying¹

Abstract

Vision-Language-Action (VLA) models have recently emerged as a promising paradigm for generalist robotic control. Built upon vision–language model (VLM) architectures, VLAs predict actions conditioned on visual observations and language instructions, achieving strong performance and generalization across tasks. However, VLAs face two major challenges: limited long-horizon context and inefficient inference due to the quadratic attention complexity and large parameter counts. Our work is motivated by the observation that much of the visual information in a trajectory remains static across timesteps (e.g., the background). Leveraging this property, we propose SD-VLA, a framework that disentangles visual inputs into multi-level static and dynamic tokens, which enables (1) retaining a single copy of static tokens across frames to significantly reduce context length, and (2) reusing the key–value (KV) cache of static tokens through a lightweight re-cache gate that updates only when necessary. This design enables efficient multi-frame integration and efficient inference. In addition, we introduce a new benchmark that more effectively evaluates the long-horizon temporal dependency modeling ability of VLAs. Experimental results show that our approach outperforms baselines on this benchmark by 39.8% absolute improvement in success rate, and achieves a 3.9% gain on the SimplerEnv benchmark. Moreover, SD-VLA delivers a 2.26 \times inference speedup over the base VLA model on the same benchmark, enabling faster and more practical real-world deployment.

1. Introduction

Vision-Language-Action (VLA) models (Li et al., 2024a; Kim et al., 2024; Qu et al., 2025; Kim et al., 2025; Zhu et al., 2024; Zhong et al., 2025; Black et al., 2024; Intelligence et al., 2025) have recently emerged as a powerful paradigm for generalist robotic control. Trained on large-scale heterogeneous datasets such as Open-X-Embodiment (Vuong et al., 2023), which aggregate expert demonstrations across diverse robotic tasks, state-of-the-art VLA models exhibit strong generalization and impressive task performance. However, state-of-the-art VLAs are typically built on top of large vision–language models (Liu et al., 2023b; Karamcheti et al., 2024; Beyer et al., 2024; Steiner et al., 2024) and face the critical challenge of high memory and computational complexity due to large parameter counts and the quadratic complexity of their contextual processing (Vaswani et al., 2017), as illustrated in Figure 1.

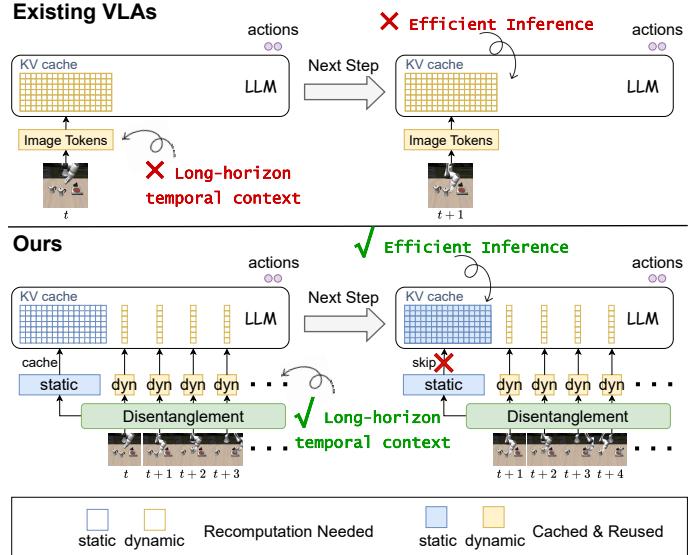


Figure 1. Our model solves two main challenges in existing VLAs with the proposed static-dynamic disentanglement. 1) By keeping one copy of static tokens across all timesteps, our model is able to squash observations of multiple steps to the model’s context; 2) By moving static tokens in front of all dynamic tokens, our model could reuse the KV-cache of previous timesteps during rollouts.

¹Department of Computer Science, Yale University. Correspondence to: Weikang Qiu <weikang.qiu@yale.edu>.

Long-horizon temporal context. Most current VLAs operate in a memoryless manner (Kim et al., 2024; Li et al., 2024a; Qu et al., 2025), taking only the current observation as input. As a result, they struggle with tasks that require temporal dependency or memory tracking. For instance, when instructed to press a button, a VLA must remember whether the button has already been pressed; otherwise, it may repeat the same action indefinitely. A straightforward solution is to include previous observations in the model input. However, modern VLM and VLA’s vision backbones typically produce hundreds of visual tokens per image, leading to prohibitively long contexts when multiple frames are concatenated for the transformer-based architecture with quadratic complexity in sequence length. Existing methods often rely on non-learnable pooling operations (Jang et al., 2025) or restrict multi-frame processing to the decoder head only (Shi et al., 2025), which either risks significant information loss or bypasses the language model’s ability to jointly reason over multiple frames.

Efficient inference. Due to their large model sizes, VLAs incur long latency for each forward pass. In real-world settings, however, robotic systems are often expected to respond promptly—for example, a household assistant should complete tasks as quickly as possible, while safety-critical scenarios such as spill containment or fire response may require near-instantaneous reactions. Moreover, recent post-training approaches for VLAs (SimpleVLA-RL Team, 2025; Lu et al., 2025), rely on reinforcement learning (Sutton et al., 1999; Schulman et al., 2017; Shao et al., 2024) and require extensive rollouts during training, making inference speed a key bottleneck. While existing work has explored improving VLA efficiency through generic techniques for general machine learning models, such as quantization, token pruning, or layer pruning (Xu et al., 2025; Yue et al., 2024; Yang et al., 2025; Kim et al., 2024), these approaches do not leverage the intrinsic characteristics of VLA tasks. Recent works (Xu et al., 2025; Liu et al., 2025; Tan et al., 2025) exploit temporal redundancy by reusing computations across consecutive frames, via KV-cache reuse or action reuse. Nonetheless, these techniques rely on heuristic, non-learnable criteria and often assume that visual similarity in pixel space indicate the temporal-consistency of their latent representations—an assumption that is invalid in transformer-based vision and language backbones, as illustrated in Figure 2.

To address these challenges, we propose SD-VLA. Our approach is motivated by a key insight: during VLA tasks, much of the visual information in a scene remains static or changes slowly over time. For example, the background of a scene, objects remaining still, or even if the objects are moved, the visual appearances remain invariant. Based on this insight, we explicitly disentangle visual tokens into dynamic tokens and multi-level static tokens with different temporal persistence. This design yields two key benefits.

First, instead of conditioning on a single image as in prior work, our model can ingest multi-step observations while maintaining a compact context: static tokens are included only once in the input sequence across timesteps, while only dynamic tokens from multiple steps are concatenated over time. This substantially reduces the effective context length and enables long-horizon modeling capability. Second, our method improves the inference efficiency by reusing key-value (KV) caches associated with static tokens from previous steps. We also introduce a recache gate module that determines whether previously cached static tokens should be reused or recomputed, which further improves performance while minimizing the inference latency.

In addition, we observe that existing benchmarks largely fail to assess a VLA’s temporal-dependency modeling capabilities. For example, tasks such as placing objects into a basket do not require remembering past trajectories. To address this gap, we design a new benchmark inspired by principles of human episodic memory, which provides a more effective evaluation of temporal reasoning and memory usage than prior benchmarks (Liu et al., 2023a; Li et al., 2024b).

To evaluate temporal-dependency modeling, we assess our model on the proposed benchmark. Our method achieves a 39.8% absolute improvement in success rate and a 29.8% improvement in heating time, indicating more powerful temporal reasoning over long horizons. To evaluate inference efficiency, we benchmark our approach on SimplerEnv and LIBERO (Liu et al., 2023a). On SimplerEnv (Li et al., 2024b), we improve the success rate by 4.9% while achieving a $2.26\times$ inference speedup. On LIBERO, we improve the success rate by 0.7% and achieve a $1.70\times$ speedup.

In summary, our contributions are as follows:

- We propose SD-VLA, which enables long-horizon memory integration and efficient inference by disentangling image tokens to dynamic tokens and multi-level static tokens with different temporal persistence.
- We introduce a trainable recache gate that adaptively determines when to refresh the cache or reuse previously cached representations, further improving the performance while minimizing the inference latency.
- We introduce LIBERO-Memory, which is a new benchmark that more effectively evaluates a VLA’s ability to model long-horizon temporal dependencies.

2. Related Works

Vision-Language-Action Models Vision-language models (VLMs) (Liu et al., 2023b; Wang et al., 2024) have demonstrated strong performance in image-related and cross-modal tasks. Leveraging these capabilities, vision-language-action (VLA) models further finetune VLMs on large-scale robotic datasets (Vuong et al., 2023; Liu et al.,

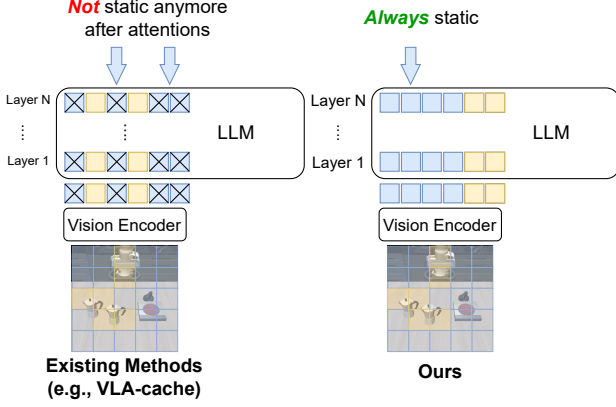


Figure 2. Some of the existing methods (Xu et al., 2025; Liu et al., 2025) that exploit to reuse information in previous frames ignore the problem that the static patches will be affected by attentions even if they are identical in the original pixel space. Unlike these methods, our model learns to disentangle and put static tokens before the dynamic tokens, making sure the static tokens will not be affected due to the causal attention mechanism of LLM backbones.

2023a), which usually consist of extensive human demonstrations. At each timestep, VLAs (Black et al., 2024; Intelligence et al., 2025; Kim et al., 2024; Li et al., 2024a; Qu et al., 2025) usually take the current environment observation (image) and a language instruction as inputs, and are trained to output actions of the next step. Although they have demonstrated high performance on certain benchmarks, due to the large parameters, they are 1) inefficient in rollout and 2) unable to incorporate historical observations in the context. In contrast, our model, by disentangling the static and dynamic components, is efficient in inference by leveraging the KV-cache of static components, and is able to incorporate a long history for temporally dependent tasks.

Acceleration for VLAs Methods to improve VLA’s efficiency usually focus on general quantization or pruning methods. For example, (Kim et al., 2024; Reddy et al., 2019; Park et al., 2024) explores quantization techniques applied to VLAs. (Shukor et al., 2025; Yang et al., 2025; Zhang et al., 2025; Yue et al., 2024) explored pruning unimportant tokens and layers according to some heuristics. Although reducing the computational complexity of VLAs, these methods just migrate acceleration methods from existing general machine learning models, thus totally ignoring the unique characteristics of VLAs. Different from these methods, recent works (Xu et al., 2025; Liu et al., 2025; Tan et al., 2025) explore temporal redundancy in decision making: consecutive frames share temporal correlation, enabling avoiding recomputation of some components by, for example, leveraging the KV-cache of previous steps. However, these methods rely on non-learnable heuristics to re-cache or simply reuse the previous action, which may suffer from suboptimal performance. Notably, some of these meth-

ods (Xu et al., 2025; Liu et al., 2025) implicitly assume that visual similarity in pixel space implies invariance in the latent representations produced by the vision encoder and LLM—an assumption that does not generally hold in transformer-based architectures, as illustrated in Figure 2.

Temporal Modeling in VLAs Existing approaches to incorporating memory or temporal context in VLAs typically rely on detecting change points (Wen et al., 2021) in visual observations or compressing historical information into compact representations. For example, Jang et al. (2025) and Liu et al. (2025) incorporate previous observations into the current input via pooling or patch-wise mixing. TraceVLA (Zheng et al., 2024) overlays visual traces of keypoints onto the current observation to indicate object trajectories. In addition, MemoryVLA (Shi et al., 2025) exposes the LLM backbone to only a single frame at each timestep and delegates multi-frame reasoning to a lightweight decoding module, which limits the model’s capacity for joint temporal decision-making. In contrast to these methods, our approach allows the LLM backbone to directly reason over multiple frames without information loss, by explicitly disentangling static and dynamic components and avoiding redundant involvement of temporally persistent visual information.

3. Method

In this section, we first present the problem formulation. We then introduce the architecture of our model, followed by the training objectives that enable static–dynamic disentanglement and the recaching mechanism. Next, we provide a computational complexity analysis and derive the theoretical acceleration and context-length improvements. Finally, we introduce the benchmark for evaluating temporal dependency modeling.

Problem Formulation Given a timestep t , the corresponding observation of the environment is denoted by \mathbf{X}_t . A VLA π predicts actions of the following steps based on previous T observations and a language instruction \mathcal{I} .

$$\pi : (\mathbf{X}_{t-T}, \mathbf{X}_{t-T+1}, \dots, \mathbf{X}_t, \mathcal{I}) \mapsto \mathbf{a}_t, \mathbf{a}_{t+1}, \dots, \quad (1)$$

where \mathbf{a}_t is the action at the t step. Current VLAs usually consider $T = 0$ due to the limited context length.

3.1. Model Architecture

Static-Dynamic disentanglement Standard VLA vision backbones typically encode the image \mathbf{X}_t into N image tokens $\mathbf{Z}_t = \mathbf{z}_{t,1}, \mathbf{z}_{t,2}, \dots, \mathbf{z}_{t,N}$ as inputs of the VLA’s LLM backbone π_{LLM} . Such a design implicitly assumes that all visual tokens must be recomputed and reprocessed at every timestep. However, real-world environments exhibit strong temporal redundancy: many visual attributes remain unchanged across time, while only a subset varies dy-

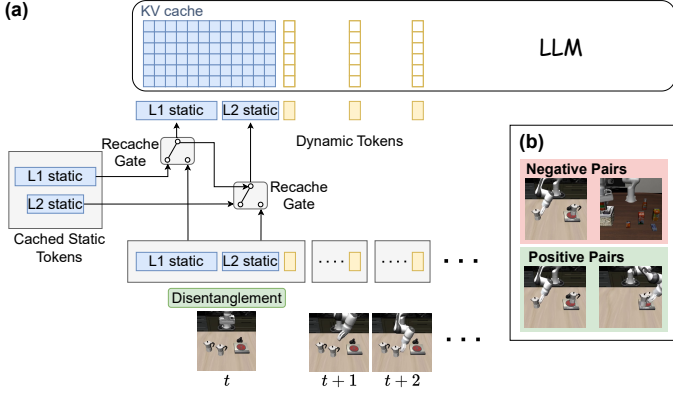


Figure 3. (a) Model architecture overview. We illustrate the design using two levels of static cache. At each level, a recache gate determines whether the cached static tokens should be reused or refreshed. If the L1 cache is refreshed, the L2 cache is also forcibly refreshed. (b) Contrastive loss used to train static tokens to be temporally persistent. Observations from the same trajectory form positive pairs, while observations from different trajectories form negative pairs.

namically. To reflect this structure, we explicitly disentangle visual tokens into static and dynamic components.

$$\mathbf{Z}_t = \mathbf{Z}_t^s, \mathbf{Z}_t^d = \underbrace{\mathbf{z}_{t,1}, \dots, \mathbf{z}_{t,N_s}}_{\text{static tokens}}, \underbrace{\mathbf{z}_{t,1}, \dots, \mathbf{z}_{t,N_d}}_{\text{dynamic tokens}} \quad (2)$$

where \mathbf{Z}_t^s are static tokens and \mathbf{Z}_t^d are dynamic tokens.

Moreover, static information itself exists at different temporal scales. For example, global scene layout or background structure may persist for long horizons, whereas object-level appearance may change more frequently due to occlusion or interaction. To capture this heterogeneity, we introduce multi-level static tokens with different temporal persistence.

The final visual inputs of VLAs could be written as

$$\mathbf{Z}_t^{s_1}, \mathbf{Z}_t^{s_2}, \dots, \mathbf{Z}_t^d = \underbrace{\mathbf{z}_{t,1}, \dots, \mathbf{z}_{t,N_{s_1}}}_{\text{static tokens (level 1)}}, \underbrace{\mathbf{z}_{t,1}, \dots, \mathbf{z}_{t,N_{s_2}}}_{\text{static tokens (level 2)}}, \dots, \underbrace{\mathbf{z}_{t,1}, \dots, \mathbf{z}_{t,N_d}}_{\text{dynamic tokens}} \quad (3)$$

where $\mathbf{Z}_t^{s_l}$ denotes static tokens at level l , and \mathbf{Z}_t^d are dynamic tokens. Dynamic tokens are recomputed at every timestep, while static tokens at each level are selectively reused through a learned caching mechanism, which will be described later.

Temporal dependency modeling Most VLAs (Kim et al., 2024; Li et al., 2024a; Qu et al., 2025) are only able to process the current observation ($T = 0$),

$$\mathbf{a}_t, \mathbf{a}_{t+1}, \dots = \pi_{\text{LLM}}(\mathbf{Z}_t), \quad (4)$$

where π_{LLM} is the LLM backbone of the VLA. With successful static-dynamic disentanglement, we only need to keep *one copy* of the static tokens within a period and construct the input from multiple observations as

$$\mathbf{a}_t, \mathbf{a}_{t+1}, \dots = \pi_{\text{LLM}}(\mathbf{Z}^{s_1}, \mathbf{Z}^{s_2}, \dots, \mathbf{Z}_{t-T}^d, \dots, \mathbf{Z}_t^d), \quad (5)$$

This formulation enables the model to leverage longer temporal context without duplicating static information, effectively alleviating context window bottlenecks while preserving all relevant visual cues.

Learning when to recache A key challenge is deciding when cached static tokens should be refreshed. Naively recomputing static tokens at every timestep negates any computational benefit, while overly aggressive reuse of static tokens risks stale representations.

To address this, we introduce a learned recache gate at each static level l

$$g_l(\mathbf{Z}_{t-\Delta}, \mathbf{Z}_t) \in [0, 1], \quad \Delta = 1, 2, \dots, T \quad (6)$$

which predicts the probability that static tokens should be recomputed given the current observation and a cached reference from Δ timesteps earlier. During training, we use the Gumbel-softmax trick (Jang et al., 2016; Maddison et al., 2016) to allow end-to-end differentiable binary decisions. At inference time, static tokens are refreshed if $g_l > \delta_l$; otherwise, the previously cache is reused. It is also worth noting that if the higher-level cache (e.g., L1) should be refreshed, the lower-level cache (e.g., L2) should also be refreshed during both training and inference. Additional details of the architecture of the recache gate could be found in Appendix B.

3.2. Training Objective

Besides the standard task loss of the underlying VLA base model $\mathcal{L}_{\text{task}}$, we introduce two additional training objectives. The first promotes temporally persistent static tokens, and the second trains the cache gate that adaptively determines when cached representations should be refreshed.

Learning static tokens To ensure that static tokens can be safely and effectively reused across time, they must remain stable over a temporal window while still encoding task-relevant information. To encourage this property, we apply a contrastive regularization term to the static tokens. Specifically, observations from different timesteps within the same trajectory are treated as positive pairs, while observations from different trajectories are treated as negative pairs. We employ the InfoNCE loss (Oord et al., 2018) $\mathcal{L}_{\text{InfoNCE}}^l$ to perform contrastive learning for static tokens at level l .

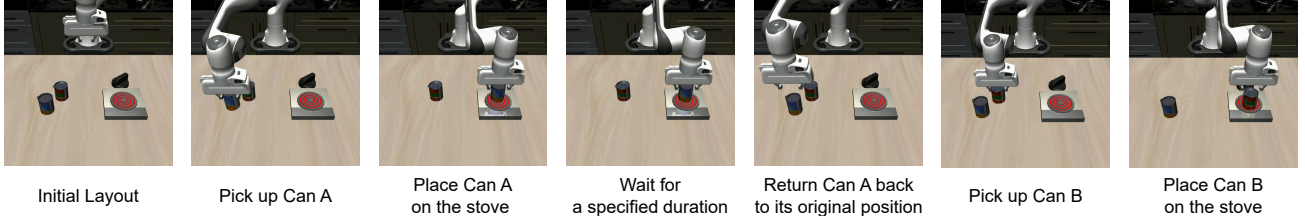


Figure 4. An example of the procedure of the proposed benchmark.

Training the recache gate If the recache gate is trained only through task supervision, it tends to recompute static tokens at every timestep, which eliminates any computational benefit. To discourage this trivial solution, we add a regularization term that biases the gate toward reuse when observations are close in time.

$$\mathcal{L}_{\text{gate}} = -p_{\Delta} \log g - (1 - p_{\Delta}) \log(1 - g) \quad (7)$$

where $p_{\Delta t} = 1 - e^{-\lambda \Delta t}$ is a predefined prior which allows the use of current observation only when Δ is large. The recache gate learns to adaptively refresh static tokens only when necessary, balancing computational efficiency and model performance.

The full training objective is

$$\mathcal{L} = \mathcal{L}_{\text{Task}} + \alpha_l \sum_l \mathcal{L}_{\text{InfoNCE}}^l + \beta \mathcal{L}_{\text{gate}}, \quad (8)$$

where α_l and β weight the auxiliary regularization terms.

3.3. Computational and Acceleration Analysis

In this subsection, we will make a computational analysis of the context length reduction and the acceleration by the introduction of the approach.

Context length Let N be the number of total tokens (including image tokens and text tokens). Let r be the fraction of tokens are cached, and $N' = (1 - r)N$ be the number of recomputed tokens.

Let T be the number of observations that should be incorporated in the context. The context length with our method reduces from NT to $rN + (1 - r)NT = NT - rN(T - 1)$.

Static token reuse The complexity of the language model backbone in the VLA model mainly comes from two types of modules: the multi-head attention (MHA) layers and the feedforward neural networks. Let d be the dimension of embedding. The FLOPs of the MHA layer are estimated by $4Nd^2 + 2N^2d$, and the FLOPs of the feedforward neural network are estimated by $2Ndm$, where m is the hidden dimension of the MLP. Therefore, the total FLOPs can be written as $F = 4Nd^2 + 2N^2d + 2Ndm$.

With our method, given that the static tokens are cached, only the dynamic parts (including the dynamic image tokens and the language instructions), the projection layers in the MHA layer will reduce to $4N'd^2$, the attention matrix calculation will reduce to $2N'Nd$, and the FLOPs of the feedforward network will reduce to $2N'dm$. The final FLOPs are $F' = 4N'd^2 + 2N'Nd + 2N'dm$.

Therefore, the theoretical FLOPs reduction of the LLM backbone *under an idealized setting* could be estimated as

$$\begin{aligned} \frac{F'}{F} &= \frac{4N'd^2 + 2N'Nd + 2N'dm}{4Nd^2 + 2N^2d + 2Ndm} \\ &= (1 - r) \frac{4d^2 + 2Nd + 2dm}{4d^2 + 2Nd + 2dm} \\ &= 1 - r \end{aligned} \quad (9)$$

The overall reduction will be diluted by the involvement of the vision backbone, the decoding module, and the cache refresh step. However, these components are significantly less computationally intensive than the LLM backbone. Moreover, the introduction of the recache gate incurs only negligible overhead ($\approx 1.27\%$) and has minimal impact on the overall computational complexity.

3.4. LIBERO-Memory Benchmark

Existing VLA benchmarks (Liu et al., 2023a; Li et al., 2024b) are designed for memoryless tasks, which do not require temporal reasoning, and the current observation alone is theoretically sufficient to predict the next action. For example, in a task with the goal “put X in the basket”, (Liu et al., 2023a) the agent can act optimally without retaining information from previous frames. As a result, it is unclear whether the reported performance of existing models for modeling temporal dependency (Jang et al., 2025; Shi et al., 2025) gains truly stem from improved temporal modeling or from other artifacts. This highlights the absence of a strong and fair benchmark for temporal dependency modeling.

To address this gap, we introduce a new benchmark designed to test memory dependency explicitly. Our benchmark includes tasks that require a robot to retain and utilize information from past observations, thereby directly evaluating a model’s temporal dependency modeling ability.

Table 1. Results on the memory-dependent tasks. All models use CogACT (Li et al., 2024a) as the base model.

Models	On Stove ↑	Position Reset ↑	Doneness ↓
TTF-VLA (Liu et al., 2025)	7.8%	1.5%	1.51
TraceVLA (Zheng et al., 2024)	2.0%	3.0%	1.41
MemoryVLA (Shi et al., 2025)	23.0%	2.0%	1.49
ContextVLA (Jang et al., 2025)	50.8%	22.3%	0.37
SD-VLA (Ours)	69.8%	83.0%	0.26

Following the setup of LIBERO, the robot operates in a tabletop environment containing three objects: two visually distinct cans and a stove. As illustrated in Figure 4, each episode consists of three tasks which reflects the structure of episodic memory (Tulving et al., 1972; Clayton & Dickinson, 1998).

Tasks Each trial consists of three tasks, each intentionally designed to require the model to retain and reason over information from previous observations at different aspects:

1. Grasp one of the cans, as specified by the instruction, and place it on the stove to heat.
2. After a period of time (given in the instruction), remove the can from the stove and return it to its original location.
3. Once the position of the first can has been restored, grasp the remaining can and place it on the stove.

This task design requires the model to retain episodic memory, integrating information about what happened, where it occurred, and when it took place (Tulving et al., 1972; Clayton & Dickinson, 1998). First, the robot must remember the initial spatial layout in order to return the first can to its original position (where). Second, it must track the elapsed time since the can was placed on the stove to determine when to remove it (when). Third, it must remember which can has already been heated in order to correctly select the remaining one for the final step (what).

These requirements prevent the task from being solved using only the current observation or a short observation history.

We use Robosuite (Zhu et al., 2025) as the simulation framework to produce the dataset. The layout and the oracle demonstrations are programmatically generated. More details of the benchmark could be found in Appendix C.

4. Experiments

In this section, we evaluate the model’s ability to capture temporal dependencies as well as its inference efficiency. We further present ablation studies of the key components of our method and analyze the model’s behavior through attention-map visualizations.

4.1. Temporal-dependency Modeling

Baselines We summarize the baseline and their strategies to incorporate memory below:

- *TTF-VLA* (Liu et al., 2025) mixes the current observation with past observations in a patch-wise manner.
- *TraceVLA* (Zheng et al., 2024) visualizes the trajectories of active points by overlaying them onto the image using distinct colors, referred to as visual traces.
- *MemoryVLA* (Shi et al., 2025) feeds the LLM backbone with images from each timestep independently and extracts a representation for each; only the multi-timestep representations are provided to the decoder.
- *ContextVLA* (Jang et al., 2025) pools historical observations into a fixed number of tokens and prepends them to the image tokens of the current observation.

Benchmark and Evaluation We adopt the proposed LIBERO-memory benchmark to evaluate memory-dependent, long-horizon tasks, whose designs are inspired by the notion of episodic memory. The benchmark comprises three objectives. (1) (*where*) *Position Reset*. After heating the first can, the robot is required to remember its original position and return it to the position. Performance is measured by success rate, where an episode is considered successful if the positional error is below a threshold. (2) (*when*) *Doneness*. The model must track the elapsed heating time and remove the can at the appropriate moment. Given a target heating duration specified in the instruction, we measure the absolute difference (in seconds) between the actual and desired heating times, capturing overcooking or undercooking. (3)(*what*) *On-Stove*. After heating and resetting the first can, the robot is required to remember which can has been cooked and place the second can on the stove for heating. We report the success rate of placing the second can on the stove.

Hyperparameter choices and implementation details We use one static level. The ratio of static tokens is set to 0.9, corresponding to 230 static tokens and 26 dynamic tokens. The number of observations is set to 20, with a sampling interval of 20 frames (1 frame per second), resulting in 750 context tokens. More details could be found in Appendix D.

Results As shown in Table 1, our method significantly

Table 2. Results on the SimplerEnv benchmark. Task suites follow the setting of Qu et al. (2025). All baselines and our method are applied to the same VLA base model (i.e., CogACT).

Method	Visual Matching			Variant Aggregation			Acceleration		
	Pick Can	Move Near	Drawer	Pick Can	Move Near	Drawer	FLOPs	Latency (ms)	Speedup
CogACT (Li et al., 2024a)	91.3	85.0	71.8	89.6	80.8	28.3	100%	1360	1.00 \times
+ FlashVLA (Tan et al., 2025)	80.0	57.1	73.6	82.5	60.8	28.6	83.4%	1024	1.33 \times
+ TTF (Liu et al., 2025)	89.3	71.3	58.4	88.0	62.7	34.0	86.5%	1051	1.29 \times
+ VLA-Cache (Xu et al., 2025)	92.0	83.3	70.5	91.7	79.3	32.5	80.1%	985	1.38 \times
+ SD-VLA (Ours)	92.7	88.8	75.0	92.4	81.0	38.9	43.4%	601	2.26\times

Table 3. Results on the LIBERO benchmark. Policy inputs: third-person image, language instruction. All baselines and our method are applied to the same VLA base model (i.e., OpenVLA-OFT).

Models	Spatial	Object	Goal	Long	Average	FLOPs	Latency (ms)	Speedup
OpenVLA-OFT (Kim et al., 2025)	96.2	98.3	96.2	90.7	95.4	100.0%	741	1.00 \times
+ FlashVLA (Tan et al., 2025)	71.8	90.0	79.2	78.8	80.0	88.7%	657	1.13 \times
+ TTF (Liu et al., 2025)	95.8	94.2	93.6	86.0	92.4	75.0%	575	1.29 \times
+ VLA-Cache (Xu et al., 2025)	95.6	92.8	94.0	89.6	93.0	85.5%	652	1.14 \times
+ SD-VLA (Ours)	97.8	97.6	96.2	92.4	96.0	63.4%	437	1.70\times

and consistently outperforms all baselines on all objectives. Single-image methods such as TraceVLA almost always fail, since the task cannot be solved from the current observation alone, and visual traces provide only marginal additional benefit. ContextVLA underperforms due to non-learnable pooling observations, which may discard critical temporal and spatial details. MemoryVLA presents the LLM backbone with only a single frame at each timestep, leaving multi-frame reasoning to a lightweight decoder; as a result, the LLM itself does not reason over multiple frames, which limits the model’s capacity. While these baselines have their own ways to reduce context length, they do so at the cost of information or model capacity. In contrast, our approach preserves all relevant visual information by reusing temporally persistent static tokens, enabling effective long-horizon reasoning within a limited context window.

4.2. Acceleration

In this study, we validate our method’s performance under acceleration by enabling KV caching of static components.

Baselines For baselines, we compare to those that also adopt temporal information reuse. *FlashVLA* (Tan et al., 2025) simply reuses the previous action based on a heuristic criterion. *TTF-VLA* (Liu et al., 2025) and *VLA-cache* (Xu et al., 2025) identify reusable visual patches using hand-designed heuristics and cache the corresponding embeddings from previous steps; however, these cached patches are not guaranteed to remain static in the hidden representation space.

Benchmark and Evaluation We use SimplerEnv (Li et al.,

2024b) and LIBERO (Liu et al., 2023a) task suite to evaluate the performance and acceleration. Kim et al. (2025) offers two settings for LIBERO, one using only a third-person image and a language instruction as inputs, and another that additionally includes an extra camera view and proprioceptive state. We adopt the former setting, as it offers broader applicability and aligns more closely with standard VLA deployment scenarios. The performance is measured by success rate, and acceleration is measured by the FLOPs reduction rate and the inference latency. Refer to Appendix A for details of the two benchmarks.

Training Dataset For the LIBERO benchmark, we simply use their corresponding training dataset, whose statistics can be found in Appendix A. For the SimplerEnv benchmark, we use Open X-Embodiment (OXE) (Vuong et al., 2023) as the training dataset, consistent with the base model. This dataset includes over 1 million real-world robotic trajectories across 60 datasets and 20 robot embodiments. The setting is consistent with the corresponding base model we use. For dataset statistics, please also refer to Appendix A.

Hyperparameter choices and implementation details We use two levels of static cache. L1 static cache consists of 133 tokens and L2 static cache consists of 107 tokens, resulting in 16 dynamic tokens. FLOPs are measured by open-source tools¹. Additional details, including the recaching threshold δ_l and the resulting average recaching intervals, could be found in Appendix D.

¹<https://github.com/MrYxJ/calculate-flops.pytorch>

Table 4. Ablation studies. *w/o Contrast* removes the contrastive learning objective during training. *w/o L2 cache* ablates the multi-level design by retaining only a single static cache level. *Fixed step* replaces the learnable recache gate by forcing the refresh of the cache at fixed intervals. The refresh interval is set to match the average recaching interval of SD-VLA (first row).

	visual matching		variant aggregation	
	PickCan	MoveNear	PickCan	MoveNear
SD-VLA	92.7	88.8	92.4	81.0
w/o Contrast	91.3	84.6	91.6	82.7
w/o L2 cache	92.0	85.0	91.5	81.5
fixed step	87.7	81.7	85.3	74.8

Results Table 2 and Table 3 summarize the performance and the acceleration results. On the SimplerEnv benchmark, our method improves the base model by 4.9%, and outperforms the best baseline by 3.9% and achieves $2.26\times$ acceleration. On the LIBERO benchmark, our method improves the base model by 0.7%, and achieves $1.70\times$ acceleration regarding the inference latency.

4.3. Ablation Studies

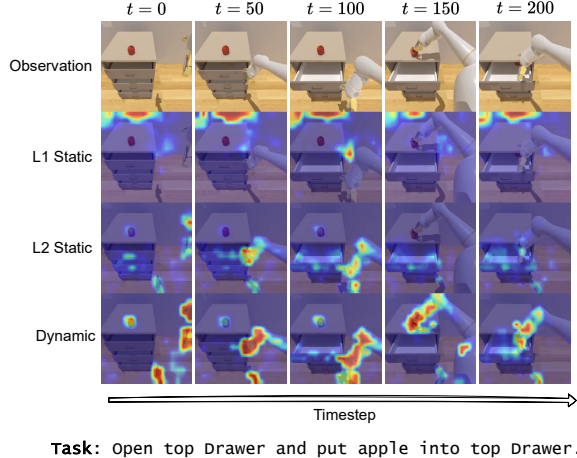
To validate the effectiveness of the proposed components, we conduct ablation studies on each of them, with results summarized in Table 4. From the second row, removing the contrastive learning objective leads to a noticeable performance degradation, as there is no longer an explicit mechanism to enforce temporal consistency in the static tokens. Performance also declines when the L2 static cache is removed and only a single-level static cache is used, as shown in the third row, highlighting the importance of the proposed multi-level caching design. Finally, replacing the learnable recache gate results in a further drop in performance, demonstrating the necessity of adaptive cache refreshing.

4.4. Visualizations

We visualize the attention map between static and dynamic tokens and the image across timesteps.

Dynamic tokens consistently attend to movable objects, most notably the gripper (including its shadow) and the apple on the tabletop. This behavior aligns with their intended role of capturing temporally varying, action-relevant elements in the scene.

L1 static tokens, which are designed to represent the most persistent visual information, primarily focus on background and ambient regions. Their attention heatmaps are often strongest in areas without salient foreground objects. We interpret this behavior as L1 static tokens of shallow layers functioning as sink tokens, capturing coarse, global scene context rather than object-specific details. Importantly, their attention patterns remain highly consistent



Task: open top Drawer and put apple into top drawer.

Figure 5. Attention map visualization across time. For each token, we compute its last-layer attention to image patches and upsample the result to the full image resolution to produce a heatmap. Heatmaps are averaged over tokens of the same type and displayed by row (e.g., the Dynamic row shows the average attention heatmap of all dynamic tokens).

across timesteps, reflecting strong temporal invariance.

L2 static tokens exhibit intermediate behavior between L1 static and dynamic tokens. They attend more strongly to semi-static objects, such as the drawer, which typically remains stationary in most of the time. At $t = 0$ both drawer handles are highlighted, as either could potentially be moved. After the drawer is opened ($t > 100$), the attention maps stabilize and remain focused on the drawer structure, indicating that these tokens capture object-level static information with moderate temporal persistence. The robotic arm is also highlighted at certain frames, which we attribute to its importance in the task and the need to preserve its appearance across timesteps.

5. Conclusion

We introduced SD-VLA, a method that improves efficiency and long-horizon reasoning in VLA models via static–dynamic disentanglement. By reusing temporally persistent static tokens and selectively refreshing them through a learnable recache gate, SD-VLA enables compact multi-frame contexts and efficient inference. Experiments show that our approach substantially improves performance on temporally dependent tasks while providing meaningful speedups over strong baselines. These results suggest that explicitly modeling temporal persistence is a promising direction for scalable and practical VLA systems.

Limitations. We realize our approach based on pretrained VLAs. Such a strategy may not fully unleash the performance of the model. Future work could focus on pretraining VLAs with our architecture and algorithm from scratch.

Impact Statement

This paper presents work whose goal is to advance the field of Machine Learning. There are many potential societal consequences of our work, none of which we feel must be specifically highlighted here.

References

Belkhale, S., Cui, Y., and Sadigh, D. Hydra: Hybrid robot actions for imitation learning. In *Proceedings of the Conference on Robot Learning (CoRL)*, 2023.

Beyer, L., Steiner, A., Pinto, A. S., Kolesnikov, A., Wang, X., Salz, D., Neumann, M., Alabdulmohsin, I., Tschanen, M., Bugliarello, E., et al. Paligemma: A versatile 3b vlm for transfer. *arXiv preprint arXiv:2407.07726*, 2024.

Black, K., Brown, N., Driess, D., Esmail, A., Equi, M., Finn, C., Fusai, N., Groom, L., Hausman, K., Ichter, B., Jakubczak, S., Jones, T., Ke, L., Levine, S., Li-Bell, A., Mothukuri, M., Nair, S., Pertsch, K., Shi, L. X., Tanner, J., Vuong, Q., Walling, A., Wang, H., and Zhilinsky, U. π_0 : A vision-language-action flow model for general robot control, 2024. URL <https://arxiv.org/abs/2410.24164>.

Brohan, A., Brown, N., Carbalaj, J., Chebotar, Y., Dabis, J., Finn, C., Gopalakrishnan, K., Hausman, K., Herzog, A., Hsu, J., et al. Rt-1: Robotics transformer for real-world control at scale. *arXiv preprint arXiv:2212.06817*, 2022.

Chen, L. Y., Adebola, S., and Goldberg, K. Berkeley UR5 demonstration dataset. <https://sites.google.com/view/berkeley-ur5/home>.

Clayton, N. S. and Dickinson, A. Episodic-like memory during cache recovery by scrub jays. *Nature*, 395(6699): 272–274, 1998.

Cui, Z. J., Wang, Y., Shafiuallah, N. M. M., and Pinto, L. From play to policy: Conditional behavior generation from uncurated robot data. In *Proceedings of International Conference on Learning Representations (ICLR)*, 2023.

Dass, S., Yapeter, J., Zhang, J., Zhang, J., Pertsch, K., Nikolaidis, S., and Lim, J. J. Clvr jaco play dataset, 2023. URL https://github.com/clvrai/clvr_jaco_play_dataset.

Ebert, F., Yang, Y., Schmeckpeper, K., Bucher, B., Georgakis, G., Daniilidis, K., Finn, C., and Levine, S. Bridge data: Boosting generalization of robotic skills with cross-domain datasets. In *Proceedings of Robotics: Science and Systems (RSS)*, 2022.

Hu, E. J., Shen, Y., Wallis, P., Allen-Zhu, Z., Li, Y., Wang, S., Wang, L., and Chen, W. Lora: Low-rank adaptation of large language models, 2021. URL <https://arxiv.org/abs/2106.09685>.

Intelligence, P., Black, K., Brown, N., Darpinian, J., Dhabalia, K., Driess, D., Esmail, A., Equi, M., Finn, C., Fusai, N., Galliker, M. Y., Ghosh, D., Groom, L., Hausman, K., Ichter, B., Jakubczak, S., Jones, T., Ke, L., LeBlanc, D., Levine, S., Li-Bell, A., Mothukuri, M., Nair, S., Pertsch, K., Ren, A. Z., Shi, L. X., Smith, L., Springenberg, J. T., Stachowicz, K., Tanner, J., Vuong, Q., Walke, H., Walling, A., Wang, H., Yu, L., and Zhilinsky, U. $\pi_{0.5}$: a vision-language-action model with open-world generalization, 2025. URL <https://arxiv.org/abs/2504.16054>.

Jang, E., Gu, S., and Poole, B. Categorical reparameterization with gumbel-softmax. *arXiv preprint arXiv:1611.01144*, 2016.

Jang, E., Irpan, A., Khansari, M., Kappler, D., Ebert, F., Lynch, C., Levine, S., and Finn, C. Bc-z: Zero-shot task generalization with robotic imitation learning. In *Proceedings of the Conference on Robot Learning (CoRL)*, 2022.

Jang, H., Yu, S., Kwon, H., Jeon, H., Seo, Y., and Shin, J. Contextvla: Vision-language-action model with amortized multi-frame context. *arXiv preprint arXiv:2510.04246*, 2025.

Kalashnikov, D., Irpan, A., Pastor, P., Ibarz, J., Herzog, A., Jang, E., Quillen, D., Holly, E., Kalakrishnan, M., Vanhoucke, V., et al. Qt-opt: Scalable deep reinforcement learning for vision-based robotic manipulation. In *Proceedings of the Conference on Robot Learning (CoRL)*, 2018.

Karamcheti, S., Nair, S., Balakrishna, A., Liang, P., Kollar, T., and Sadigh, D. Prismatic vlms: Investigating the design space of visually-conditioned language models. In *Forty-first International Conference on Machine Learning*, 2024.

Kim, M. J., Pertsch, K., Karamcheti, S., Xiao, T., Balakrishna, A., Nair, S., Rafailov, R., Foster, E., Lam, G., Sanketi, P., et al. Openvla: An open-source vision-language-action model. *arXiv preprint arXiv:2406.09246*, 2024.

Kim, M. J., Finn, C., and Liang, P. Fine-tuning vision-language-action models: Optimizing speed and success. *arXiv preprint arXiv:2502.19645*, 2025.

Li, Q., Liang, Y., Wang, Z., Luo, L., Chen, X., Liao, M., Wei, F., Deng, Y., Xu, S., Zhang, Y., et al. Cogact: A

foundational vision-language-action model for synergizing cognition and action in robotic manipulation. *arXiv preprint arXiv:2411.19650*, 2024a.

Li, X., Hsu, K., Gu, J., Pertsch, K., Mees, O., Walke, H. R., Fu, C., Lunawat, I., Sieh, I., Kirmani, S., et al. Evaluating real-world robot manipulation policies in simulation. *arXiv preprint arXiv:2405.05941*, 2024b.

Liu, B., Zhu, Y., Gao, C., Feng, Y., Liu, Q., Zhu, Y., and Stone, P. Libero: Benchmarking knowledge transfer for lifelong robot learning. *Advances in Neural Information Processing Systems*, 36:44776–44791, 2023a.

Liu, C., Zhang, J., Li, C., Zhou, Z., Wu, S., Huang, S., and Duan, H. Ttf-vla: Temporal token fusion via pixel-attention integration for vision-language-action models. *arXiv preprint arXiv:2508.19257*, 2025.

Liu, H., Li, C., Wu, Q., and Lee, Y. J. Visual instruction tuning. *Advances in neural information processing systems*, 36:34892–34916, 2023b.

Liu, H., Nasiriany, S., Zhang, L., Bao, Z., and Zhu, Y. Robot learning on the job: Human-in-the-loop autonomy and learning during deployment. In *Proceedings of Robotics: Science and Systems (RSS)*, 2023c.

Loshchilov, I. and Hutter, F. Decoupled weight decay regularization, 2019. URL <https://arxiv.org/abs/1711.05101>.

Lu, G., Guo, W., Zhang, C., Zhou, Y., Jiang, H., Gao, Z., Tang, Y., and Wang, Z. Vla-rl: Towards masterful and general robotic manipulation with scalable reinforcement learning. *arXiv preprint arXiv:2505.18719*, 2025.

Luo, J., Xu, C., Geng, X., Feng, G., Fang, K., Tan, L., Schaal, S., and Levine, S. Multi-stage cable routing through hierarchical imitation learning. *IEEE Transactions on Robotics*, 40:1476–1491, 2024a.

Luo, J., Xu, C., Liu, F., Tan, L., Lin, Z., Wu, J., Abbeel, P., and Levine, S. Fmb: a functional manipulation benchmark for generalizable robotic learning. *The International Journal of Robotics Research*, 2024b.

Maddison, C. J., Mnih, A., and Teh, Y. W. The concrete distribution: A continuous relaxation of discrete random variables. *arXiv preprint arXiv:1611.00712*, 2016.

Mandlekar, A., Zhu, Y., Garg, A., Booher, J., Spero, M., Tung, A., Gao, J., Emmons, J., Gupta, A., Orbay, E., et al. Roboturk: A crowdsourcing platform for robotic skill learning through imitation. In *Proceedings of the Conference on Robot Learning (CoRL)*, 2018.

Mees, O., Borja-Diaz, J., and Burgard, W. Grounding language with visual affordances over unstructured data. In *Proceedings of the IEEE International Conference on Robotics and Automation (ICRA)*, 2023.

Mendonca, R., Bahl, S., and Pathak, D. Structured world models from human videos. In *Proceedings of the Conference on Robot Learning (CoRL)*, 2023.

Nasiriany, S., Gao, T., Mandlekar, A., and Zhu, Y. Learning and retrieval from prior data for skill-based imitation learning. In *Proceedings of the Conference on Robot Learning (CoRL)*, 2023.

Oord, A. v. d., Li, Y., and Vinyals, O. Representation learning with contrastive predictive coding. *arXiv preprint arXiv:1807.03748*, 2018.

Park, S., Kim, H., Jeon, W., Yang, J., Jeon, B., Oh, Y., and Choi, J. Quantization-aware imitation-learning for resource-efficient robotic control, 2024. URL <https://arxiv.org/abs/2412.01034>.

Qu, D., Song, H., Chen, Q., Yao, Y., Ye, X., Ding, Y., Wang, Z., Gu, J., Zhao, B., Wang, D., et al. Spatialvla: Exploring spatial representations for visual-language-action model. *arXiv preprint arXiv:2501.15830*, 2025.

Quere, G., Hagengruber, A., Iskandar, M., Bustamante, S., Leidner, D., Stulp, F., and Vogel, J. Shared control templates for assistive robotics. In *Proceedings of the IEEE International Conference on Robotics and Automation (ICRA)*, 2020.

Reddy, S., Dragan, A. D., and Levine, S. Sqil: Imitation learning via reinforcement learning with sparse rewards, 2019. URL <https://arxiv.org/abs/1905.11108>.

Rosete-Beas, E., Mees, O., Kalweit, G., Boedecker, J., and Burgard, W. Latent plans for task-agnostic offline reinforcement learning. In *Proceedings of the Conference on Robot Learning (CoRL)*, 2022.

Saxena, S., Sharma, M., and Kroemer, O. Multi-resolution sensing for real-time control with vision-language models. In *Proceedings of the Conference on Robot Learning (CoRL)*, 2023.

Schulman, J., Wolski, F., Dhariwal, P., Radford, A., and Klimov, O. Proximal policy optimization algorithms. *arXiv preprint arXiv:1707.06347*, 2017.

Shah, R., Martín-Martín, R., and Zhu, Y. Mutex: Learning unified policies from multimodal task specifications. In *Proceedings of the Conference on Robot Learning (CoRL)*, 2023.

Shao, Z., Wang, P., Zhu, Q., Xu, R., Song, J., Bi, X., Zhang, H., Zhang, M., Li, Y., Wu, Y., et al. Deepseekmath: Pushing the limits of mathematical reasoning in open language models. *arXiv preprint arXiv:2402.03300*, 2024.

Shi, H., Xie, B., Liu, Y., Sun, L., Liu, F., Wang, T., Zhou, E., Fan, H., Zhang, X., and Huang, G. Memoryvla: Perceptual-cognitive memory in vision-language-action models for robotic manipulation, 2025. URL <https://arxiv.org/abs/2508.19236>.

Shukor, M., Aubakirova, D., Capuano, F., Kooijmans, P., Palma, S., Zouitine, A., Aractingi, M., Pascal, C., Russi, M., Marafioti, A., Alibert, S., Cord, M., Wolf, T., and Cadene, R. Smolvla: A vision-language-action model for affordable and efficient robotics, 2025. URL <https://arxiv.org/abs/2506.01844>.

SimpleVLA-RL Team. Simplevla-rl: Online rl with simple reward enables training vla models with only one trajectory. <https://github.com/PRIME-RL/SimpleVLA-RL>, 2025. GitHub repository.

Steiner, A., Pinto, A. S., Tschannen, M., Keysers, D., Wang, X., Bitton, Y., Gritsenko, A., Minderer, M., Sherbondy, A., Long, S., et al. Paligemma 2: A family of versatile vlms for transfer. *arXiv preprint arXiv:2412.03555*, 2024.

Sutton, R. S., McAllester, D., Singh, S., and Mansour, Y. Policy gradient methods for reinforcement learning with function approximation. *Advances in neural information processing systems*, 12, 1999.

Tan, X., Yang, Y., Ye, P., Zheng, J., Bai, B., Wang, X., Hao, J., and Chen, T. Think twice, act once: Token-aware compression and action reuse for efficient inference in vision-language-action models. *arXiv preprint arXiv:2505.21200*, 2025.

Tulving, E. et al. Episodic and semantic memory. *Organization of memory*, 1(381-403):1, 1972.

Vaswani, A., Shazeer, N., Parmar, N., Uszkoreit, J., Jones, L., Gomez, A. N., Kaiser, Ł., and Polosukhin, I. Attention is all you need. *Advances in neural information processing systems*, 30, 2017.

Vuong, Q., Levine, S., Walke, H. R., Pertsch, K., Singh, A., Doshi, R., Xu, C., Luo, J., Tan, L., Shah, D., et al. Open x-embodiment: Robotic learning datasets and rt-x models. In *Towards Generalist Robots: Learning Paradigms for Scalable Skill Acquisition@ CoRL2023*, 2023.

Walke, H., Black, K., Lee, A., Kim, M. J., Du, M., Zheng, C., Zhao, T., Hansen-Estruch, P., Vuong, Q., He, A., Myers, V., Fang, K., Finn, C., and Levine, S. Bridgedata v2: A dataset for robot learning at scale. In *Proceedings of the Conference on Robot Learning (CoRL)*, 2023.

Wang, W., Lv, Q., Yu, W., Hong, W., Qi, J., Wang, Y., Ji, J., Yang, Z., Zhao, L., XiXuan, S., et al. Cogvlm: Visual expert for pretrained language models. *Advances in Neural Information Processing Systems*, 37:121475–121499, 2024.

Wen, C., Lin, J., Qian, J., Gao, Y., and Jayaraman, D. Keyframe-focused visual imitation learning, 2021. URL <https://arxiv.org/abs/2106.06452>.

Xu, S., Wang, Y., Xia, C., Zhu, D., Huang, T., and Xu, C. Vla-cache: Towards efficient vision-language-action model via adaptive token caching in robotic manipulation. *arXiv preprint arXiv:2502.02175*, 2025.

Yan, G., Wu, K., and Wang, X. ucsd kitchens dataset. https://github.com/geyan21/rlds_dataset_builder/tree/main/ucsd_kitchens, 2023.

Yang, Y., Wang, Y., Wen, Z., Zhongwei, L., Zou, C., Zhang, Z., Wen, C., and Zhang, L. Efficientvla: Training-free acceleration and compression for vision-language-action models. *arXiv preprint arXiv:2506.10100*, 2025.

Yue, Y., Wang, Y., Kang, B., Han, Y., Wang, S., Song, S., Feng, J., and Huang, G. Deer-vla: Dynamic inference of multimodal large language models for efficient robot execution. *Advances in Neural Information Processing Systems*, 37:56619–56643, 2024.

Zhang, R., Dong, M., Zhang, Y., Heng, L., Chi, X., Dai, G., Du, L., Du, Y., and Zhang, S. Mole-vla: Dynamic layer-skipping vision language action model via mixture-of-layers for efficient robot manipulation. *arXiv preprint arXiv:2503.20384*, 2025.

Zheng, R., Liang, Y., Huang, S., Gao, J., Daumé III, H., Kolobov, A., Huang, F., and Yang, J. Tracevla: Visual trace prompting enhances spatial-temporal awareness for generalist robotic policies. *arXiv preprint arXiv:2412.10345*, 2024.

Zhong, Y., Bai, F., Cai, S., Huang, X., Chen, Z., Zhang, X., Wang, Y., Guo, S., Guan, T., Lui, K. N., Qi, Z., Liang, Y., Chen, Y., and Yang, Y. A survey on vision-language-action models: An action tokenization perspective, 2025. URL <https://arxiv.org/abs/2507.01925>.

Zhou, G., Dean, V., Srirama, M. K., Rajeswaran, A., Pari, J., Hatch, K., Jain, A., Yu, T., Abbeel, P., Pinto, L., et al. Train offline, test online: A real robot learning benchmark. In *Proceedings of the IEEE International Conference on Robotics and Automation (ICRA)*, 2023.

Zhu, X., Tian, R., Xu, C., Huo, M., Zhan, W., Tomizuka, M., and Ding, M. Fanuc manipulation: A dataset for learning-based manipulation with fanuc

mate 200id robot. <https://sites.google.com/berkeley.edu/fanuc-manipulation>, 2023a.

Zhu, X., Li, J., Liu, Y., Ma, C., and Wang, W. A survey on model compression for large language models, 2024. URL <https://arxiv.org/abs/2308.07633>.

Zhu, Y., Stone, P., and Zhu, Y. Bottom-up skill discovery from unsegmented demonstrations for long-horizon robot manipulation. *IEEE Robotics and Automation Letters*, 7(2):4126–4133, 2022.

Zhu, Y., Joshi, A., Stone, P., and Zhu, Y. Viola: Imitation learning for vision-based manipulation with object proposal priors. In *Proceedings of the Conference on Robot Learning (CoRL)*, 2023b.

Zhu, Y., Wong, J., Mandlekar, A., Martín-Martín, R., Joshi, A., Lin, K., Maddukuri, A., Nasiriany, S., and Zhu, Y. robosuite: A modular simulation framework and benchmark for robot learning, 2025. URL <https://arxiv.org/abs/2009.12293>.

A. Dataset Details

A.1. Training

Table 5 summarizes the Open-X-Embodiment dataset we use for the base model CogACT (Li et al., 2024a). Table 6 summarizes the LIBERO dataset we use for the base model OpenVLA-OFT (Kim et al., 2025).

Table 5. Open-X-Embodiment dataset composition we use for CogACT training.

Dataset	Ratio
Fractal (Brohan et al., 2022)	27.1%
Kuka (Kalashnikov et al., 2018)	14.7%
Bridge (Walke et al., 2023; Ebert et al., 2022)	15.3%
Taco Play (Rosete-Beas et al., 2022; Mees et al., 2023)	3.4%
Jaco Play (Dass et al., 2023)	0.6%
Berkeley Cable Routing (Luo et al., 2024a)	0.3%
Roboturk (Mandlekar et al., 2018)	2.7%
Viola (Zhu et al., 2023b)	1.1%
Berkeley Autolab UR5 (Chen et al.)	1.4%
Toto (Zhou et al., 2023)	2.3%
Stanford Hydra Dataset (Belkhale et al., 2023)	5.1%
Austin Buds Dataset (Zhu et al., 2022)	0.2%
NYU Franka Play Dataset (Cui et al., 2023)	1.0%
UCSD Kitchen Dataset (Yan et al., 2023)	<0.1%
Austin Sailor Dataset (Nasiriany et al., 2023)	2.5%
Austin Sirius Dataset (Liu et al., 2023c)	2.0%
DLR EDAN Shared Control (Quere et al., 2020)	<0.1%
IAMLab CMU Pickup Insert (Saxena et al., 2023)	1.0%
UTAustin Mutex (Shah et al., 2023)	2.6%
Berkeley Fanuc Manipulation (Zhu et al., 2023a)	0.9%
CMU Stretch (Mendonca et al., 2023)	0.2%
BC-Z (Jang et al., 2022)	8.6%
FMB Dataset (Luo et al., 2024b)	2.4%

Table 6. LIBERO dataset

Dataset	Libero-Spatial	Libero-Object	Libero-Goal	Libero-Long
#(trajectories)	432	454	428	379

A.2. Evaluation

SimplerEnv SimplerEnv (Li et al., 2024b) is a simulation-based benchmark designed for tabletop robotic manipulation. It is explicitly constructed to minimize the sim-to-real gap, demonstrating strong alignment between simulation performance and real-world execution across multiple robot platforms. The benchmark supports two complementary evaluation configurations: Visual Matching, which emphasizes high visual fidelity to real-world environments, and Variant Aggregations, which systematically introduce visual perturbations such as changes in background, lighting, distractors, and surface textures to assess robustness. SIMPLER includes tasks instantiated on both the Google Robot and the WidowX robot, covering a diverse set of manipulation primitives such as picking, placing, navigation, and articulated object interaction. In all tasks, agents receive RGB visual observations and natural language instructions. SIMPLER offers two evaluation settings:

- *Visual Matching*: Real-world images are overlaid onto simulated environments, with foreground objects and robots adjusted to closely match real-world appearances.
- *Variant Aggregation*: Multiple environmental variations are generated—such as different backgrounds, lighting conditions, and surface textures.

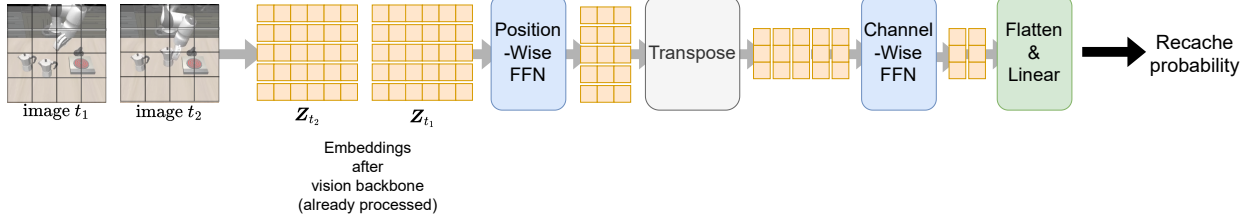


Figure 6. Architecture of the recache gate.

LIBERO LIBERO is built around a simulated Franka Emika Panda arm and provides high-quality human-teleoperated demonstration data paired with language-conditioned tasks to support sample-efficient learning and generalization. The benchmark comprises four distinct task suites—LIBERO-Spatial, LIBERO-Object, LIBERO-Goal, and LIBERO-Long, each providing 10 distinct tasks.

B. Architecture Details

Reache gate The recache gate is designed to predict the probability of refreshing cached representations based on images (or their latent representations) observed at different timesteps. To minimize additional inference latency in the VLA, the recache gate must remain lightweight. Accordingly, we adopt a simple MLP-based architecture.

As illustrated in Figure 6, the gate takes as input latent embeddings Z_{t_1} and Z_{t_2} produced by the VLA’s vision backbone at two different timesteps. We first apply a position-wise feedforward network to each embedding. The embeddings are then transposed to enable a channel-wise feedforward operation. After these transformations and dimensionality reduction, the resulting features are flattened and passed through a final MLP to predict the recache probability. For different static levels, we share all parameters except for the final prediction head.

C. LIBERO-Memory Benchmark

Following the LIBERO benchmark (Liu et al., 2023a), the layout initialization is specified by the BDDL scene description file, which is a file format that specifies the initial layout’s sampling strategy and other meta information.

```

1 (define (problem LIBERO_Kitchen_Tabletop_Manipulation)
2   (:domain robosuite)
3   (:language Heat the tomato sauce on the stove for 1.4 second and then heat the alphabet
4     soup)
5   (:regions
6     (operation_region
7       (:target kitchen_table)
8       (:ranges (
9         (-0.2 0.09999999999999999 0.0 0.2)
10        )
11       (:yaw_rotation (
12         (0.0 0.0)
13        )
14       )
15     )
16     (stove_region
17       (:target kitchen_table)
18       (:ranges (
19         (-0.3000000000000004 -0.2 -0.1 -0.0999999999999999)
20        )
21       (:yaw_rotation (
22         (0.0 0.0)
23        )
24       )
25     )
26   )

```

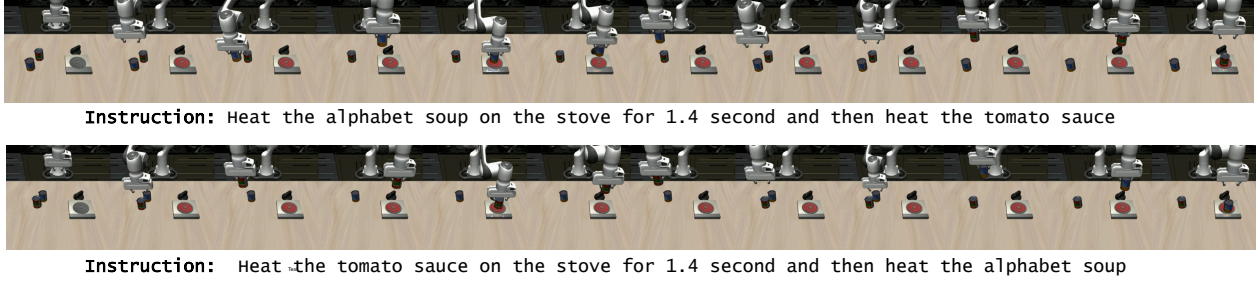


Figure 7. Examples of our proposed LIBERO Memory Benchmark.

```

27   (:cook_region
28     (:target flat_stove_1)
29   )
30 )
31
32 (:fixtures
33   kitchen_table - kitchen_table
34   flat_stove_1 - flat_stove
35 )
36
37 (:objects
38   alphabet_soup_1 - alphabet_soup
39   tomato_sauce_1 - tomato_sauce
40 )
41
42 (:obj_of_interest
43   tomato_sauce_1
44   alphabet_soup_1
45 )
46
47 (:init
48   (On tomato_sauce_1 kitchen_table_operation_region)
49   (On alphabet_soup_1 kitchen_table_operation_region)
50   (On flat_stove_1 kitchen_table_stove_region)
51   (TurnOn flat_stove_1)
52 )
53
54 (:goal
55   (And (CloseXY tomato_sauce_1) (On alphabet_soup_1 flat_stove_1_cook_region)))
56 )
57 )
58

```

Listing 1. An example of the PDDL scene description file used in LIBERO-Memory.

Oracle demonstrations We generate expert trajectories programmatically because the correct behavior in LIBERO-Memory is fully specified and unambiguous. For example, for a sub-task such as “place the tomato sauce can on the stove”, an oracle with access to the simulator state can deterministically execute the correct sequence. The oracle knows the target object and its current location, and issues movement commands that drive the end-effector toward that location. After each movement, it compares the updated end-effector position with the desired target and decides the next control direction. Once the end-effector is sufficiently close, the oracle closes the gripper to grasp the object and subsequently moves it to the specified target location.

Figure 7 shows more detailed example trajectories of the benchmark. Figure 8 shows the distribution of the trajectory length of the benchmark.

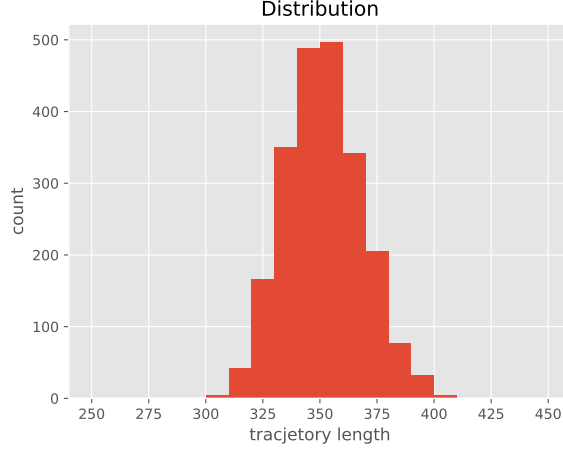


Figure 8. Distribution of the trajectory length of the LIBERO-Memory benchmark

D. Implementation Details and Hyperparameter Choices

For the recache gate in Figure 6, the first FFN is a 3-layer MLP that reduce the embedding dimension from 2×4096 to 128. The second FFN is a 3-layer MLP that reduce the number of embeddings from 256 to 128. The head after the flatten operation is a linear layer with input dimension 128×64 .

CogACT We use LoRA (Hu et al., 2021) to train the model, with the rank of 32. We use AdamW (Loshchilov & Hutter, 2019) with a learning rate of 2×10^{-5} . Training is conducted on $2 \times$ H100 for 6000 steps, with a global batch size of 32.

OpenVLA-OFT We use LoRA (Hu et al., 2021) to train the model, with the rank of 32. We use AdamW (Loshchilov & Hutter, 2019) with a learning rate of 5×10^{-4} . Training is conducted on $2 \times$ H100 for 15000 steps, with a global batch size of 64.

For both base models, the coefficients of the training objectives are set as $\alpha_1 = 0.2, \alpha_2 = 0.1, \beta = 0.1$. For their corresponding benchmarks, the evaluation and the acceleration measurements are all conducted on $1 \times$ L40S for each task.

Table 7 summarizes the recaching threshold settings and the resulting average recaching intervals.

Table 7. Recaching threshold settings and the resulting average recaching intervals

	Pick Can	Move Near	Drawer
δ_1	0.8	0.4	0.7
δ_2	0.4	0.3	0.4
avg interval of L1	9.14	2.23	7.47
avg interval of L2	2.15	2.05	4.16